Journal of Nuclear Materials 532 (2020) 152050

Contents lists available at ScienceDirect

Journal of Nuclear Materials

journal homepage: www.elsevier.com/locate/jnucmat

Dependence of thermal conductivity on fission-product defects and vacancy concentration in thorium dioxide

M.J. Rahman [a, *], B. Szpunar [b], J.A. Szpunar [a]

[a] Dept of Mechanical Engineering, University of Saskatchewan, 57 Campus Drive, Saskatoon, SK, S7N 5A9, Canada
[b] Dept of Physics and Engineering Physics, University of Saskatchewan, 116 Science Place, Saskatoon, SK, S7N 5E2, Canada

ARTICLE INFO

Article history:
Received 23 September 2019
Received in revised form
18 January 2020
Accepted 10 February 2020
Available online 14 February 2020

Keywords:
Thorium dioxide
Specific heat
Thermal conductivity
Fission products
Vacancy concentration
Molecular dynamics

ABSTRACT

The dependence of thermal conductivity on fission generated products (FPs) and vacancies in ThO_2 within the temperature range 300–1500 K has been investigated using molecular dynamics (MD) simulations. The effect of defect on specific heat and enthalpy increment is also studied. Two typical FPs: Xe and Kr (0–1.02% defect) and vacancies with 0–5% concentration are examined. The relative change in enthalpy increment due to defects is small (<2%) for lower concentration at all temperatures; however, for higher defect concentration, this parameter decreases with temperature. The vacancies reduce specific heat in the low temperature range, while the reduction is negligible at elevated temperature. In contrast, considering all temperatures, a maximum of ~2% reduction in specific heat is observed for ThO_2-FP systems with any concentration of defect. Thermal conductivity of ThO_2 degrades significantly by the FPs and vacancies and the degradation decreases with the increase in temperature. For both pure and defective ThO_2, the scattering parameters are derived by fitting a Callaway and Analytical model to MD data. The percentage of reduction (R) by defects in thermal conductivity follows the trend $R_{FP} > R_{Vacancy}$, where R_{Xe} is somewhat higher than R_{Kr} for the studied concentrations of FPs. The reduction rate is higher for the systems with smaller concentration of defect and vice versa. Our results report that the degree of reduction in conductivity of defected ThO_2 is lower compared to that of UO_2. We also observed that the clustered defects reduce thermal conductivity more than that by individually distributed defects and conductivity decreases almost linearly with the increase in cluster size.

1. Introduction

For safe reactor operation, the heat generated from fission events is required to be transported efficiently. Thermal conductivity (κ) is the most important thermal property of nuclear fuel that controls the heat removal, and eventually the electricity production. Fuel performance codes, that take into account all the complex phenomena, such as fission-gas release, radiation damage, microstructural changes, also largely depend on the conductivity of fuel materials to demonstrate their behavior and failure under operation [1–3]. In nuclear process, the properties and performance of fuel materials are severely deteriorated due to irradiation. In particular, radiation induced fission products (FPs) and vacancies produce bubbles and voids and therefore cause fuel swelling and fragmentation [4,5]. Moreover, reduction in thermal conductivity, because of the trapped inert gases in fuel-cladding gap, increases the temperature of the fuel and therefore builds pressure on the cladding tube [6]. Therefore, in order to characterize thermal transfer behavior of irradiated fuel, it is of great interest to investigate the effect of fission product and vacancy on the thermal conductivity of fuel material.

Besides traditional Urania (UO_2), thoria (ThO_2) has been used as alternative nuclear fuel over the years. Greater burn-ups and higher concentration of thorium (2–10%) makes ThO_2 energy efficient and highly economical [7]. Thorium is 3–4 times more available than uranium in the earth crust [8,9]. Since thoria has higher thermal conductivity and higher melting point than UO_2, it is a potential candidate as a fuel for safer reactors [10]. Due to its importance, thermal and mechanical properties of ThO_2 have been reported in a number of studies [11–23]. However, none of these studies investigates the influence of fission-generated products on thermal transport characteristics in $ThO_2$and therefore no relevant literature is available.

* Corresponding author.
E-mail address: jahid008@gmail.com (M.J. Rahman).

https://doi.org/10.1016/j.jnucmat.2020.152050
0022-3115/

As a conventional nuclear fuel, UO_2 has been investigated in few studies to understand the impact of fission products, porosities and other defects on the thermal transport behavior [24–28]. In an experimental investigation of porous UO_2 with 5 different porosity levels varied from 4.11 to 8.58% (volume fraction), Hobson et al. showed that reduction in thermal conductivity depends on temperature and the porosity correction is described by analytical functions [24]. Experimental study on the effects of soluble fission products (Sr, Zr, Y, La, Ce, Nd) in UO_2-based fuel reported a decrease in κ with increasing concentration of FPs at low temperature, in contrast, this dependence is nearly negligible at high temperature [25]. The authors also concluded that the heat transfer process in UO_2 is governed by phonon-phonon and phonon-defect scattering in low and high FPs content respectively.

In addition to experimental studies [24,25], computational works [26–34] also contributed an important role on understanding the effect of FPs and porosities in UO_2. For thermal transport study in nuclear fuel, atomistic simulations are very effective since thermo-physical and thermo-mechanical properties are strongly controlled by the atomic scale mechanisms. Using Density Functional Theory (DFT) simulation, a detailed study of energetics of Xe and Kr fission gases and their clusters in thoria is reported by Kuganathan et al. [26]. In a 3-D finite-element simulation of porous UO_2 with0–30 vol% spherical porosity and pore size of 70–172 μm, Yun and Stan showed a nonlinear increase in centerline temperature with porosity content [27]. However, pore size distribution weakly controls the thermal transport behavior [27]. An analytical study of phonon driven thermal conductivity in porous UO_2 demonstrated a decrease in κ due to porosity, which is mostly attributed to the reduced mean free path in porous system [28]. In addition, Liu at al studied the effect of uranium, oxygen and FP defects (Xe, Zr, La) on thermal transport in UO_2 using atomistic simulations [29]. A greater decrease in thermal conductivity is observed for Xe, in comparison to that of Zr and La. The authors also reported higher reduction in κ by U-defects than O-defects [29]. Recently, in a thermal transport study for porous ThO_2, Park et al. [30] observed a stronger effect on reduction of conductivity by Th-vacancy compared to that by O-vacancy. An influence of system size on MD derived thermal conductivity in porous ThO_2 is shown by Malakkal et al. [31]. In another MD study, the relative impact of U and Pu doping on thermal properties of ThO_2 has been described by Ma et al. [19]. Particularly, thermophysical property of Pu doped ThO_2 is reported by Galvin and his co-workers [32]. Moreover, Ghosh et al. [33] and Somayajulu et al. [34] studied the effect of Ce and Pu doping, respectively, on thermal expansion and thermal conductivity.

To date, very few studies investigate the effect of fission product defects and vacancies on the thermal conductivity in $ThO_2$and therefore thermal transfer behavior is not well understood for this alternative fuel. The reduction in thermal conductivity of ThO_2 by typical fission products and fuel vacancy is examined in our study using MD simulations. This investigation can contribute to parameterize the fuel performance code for developing better understanding of thermal properties of irradiated ThO_2 fuel. For accurate atomic description and reliable MD results, a many-body interatomic potential developed by Cooper, Rushton and Grimes (CRG) [35] is adopted. In addition, a complementary potential set is utilized to incorporate Xe and Kr atoms in ThO_2 [36].

In this work, molecular dynamics (MD) simulations have been performed to investigate the effect of fission product (FP) and vacancy on the thermal conductivity and specific heat in ThO_2. Two typical FPs: xenon (Xe) and krypton (Kr) are considered in a range of temperature from 300 to 1500 K. Enthalpy increment and specific heat of pure and defected ThO_2 is calculated relative to the enthalpy of 300 K. Thermal conductivities of all studied systems are presented in analytical form, which is applicable in fuel performance codes. The reduction in κ of defected ThO_2 is compared with the counterpart of UO_2. Attention has also been paid to the distribution of FPs and vacancies and their influence on the fuel conductivity.

2. Computational method

In this study, MD simulations are carried out using LAMMPS (Large-scale Atomic/Molecular Massively Parallel Simulator) code [37,38]. The interatomic force between the actinides and oxygen are described by a many-body potential developed by Cooper et al. [35]. A complementary set of parameters is used for the interactions of Xe and Kr atoms within actinide oxides [36]. The temperature range we use varies from 300 to 1500 K at every 300 K. In order to create stress free structure, equilibrium lattice parameter has been used at each temperature.

The FP-defected ThO_2 structure were generated by inserting Xe and Kr atoms at Schottky-vacancy sites, where one U vacancy and two O vacancies bound together. Previous studies have shown that the bound Schottky defects are the most energetically favorable sites for the fission gases to be accommodated [29,39]. The vacancies in ThO_2 structure are created by removing Th and O_2 atoms from both cation and anion substitutional lattice positions [21]. To investigate the effect of different level of defect concentration, ThO_2 structures are generated with 0.34%, 0.68%, 1.02% FPs and 1%, 2%, 5% vacancies. Both the FPs and vacancies are distributed along the direction of heat transfer to confirm their interaction and impact on the thermal transport behavior. We also examined the influence of defect distribution on thermal conductivity. In addition to individual defect of FP or vacancy, we insert 6, 12, 18, 24 defect atoms together in close proximity of each other at different Schottky defect positions to form clustered defect maintaining the same composition. The effect of cluster size on thermal transfer has been studied.

For thermal conductivity measurement, rectangular supercells with 5×5 unit cell cross section are used. Conductivity calculation depends very weakly on the cross sectional area [20,40] and therefore throughout the investigation we used the same area for all simulation cells. However, a wide range of dimensions has been used in the direction of thermal transport. The supercells are generated with 5 different lengths, such as 36, 44, 60, 90 and 200 unit cells. Different lengths of super cell are useful to examine the system size dependence on thermal conductivity and determine the bulk value.

The super cells are initially equilibrated using an NPT (i.e., constant number of atoms, pressure and temperature) ensemble at zero external pressure. The equilibration is confirmed by a steady state in the energy and volume of the system. The equilibrated structures are then used for thermal conductivity measurement. A time step of 1fs is used throughout the simulation. Periodic boundary conditions are employed in all directions.

Thermal conductivity is calculated using a non-equilibrium MD technique, Muller-Plathe approach [41]. In this method, the supercell is split into 20 bins in z-axis, along which a constant heat flux is imposed by swapping the atoms between central and edge bins. The continuous exchange of thermal energy creates a temperature gradient between the two extreme bins (hot and cold). Eventually, the transferred kinetic energy becomes equal to the applied heat flux and the temperature gradient reaches a steady state. A linear response in the temperature profile is confirmed after 1000 ps of heat flow induction. From the average temperature gradient, the thermal conductivity was calculated using the following expression:

$$\kappa = -\frac{J_z}{\frac{\partial T}{\partial z}} = -\frac{KE_z}{2tL_xL_y}\frac{1}{\frac{\partial T}{\partial z}} \quad (1)$$

where, J_z is the applied heat flux in z-direction and KE_z refers to the amount of total transferred kinetic energy that is calculated over the course of simulation time t. L_x and L_y are the supercell lengths of that forms the cross sectional area through which the heat is transported. $<\partial T/\partial z>$ represents the time averaged temperature gradient.

3. Thermal conductivity fitting models

3.1. Analytical model

In order to develop performance model of nuclear fuel, thermal conductivity is required to be described using analytical expression. In general, these formulations are expressed in terms of a proportional relationship between κ and temperature dependent phonon mean free path [15,29]. For pure ThO_2, the description of thermal conductivity is as follows:

$$\kappa = \frac{1}{A + BT} \quad (2)$$

where, T is the temperature, A and B are fitting parameters that represent the effect of phonon-phonon scattering on thermal conductivity in pure system.

For defected ThO_2, Equation (2) has been modified by adding extra term to account the effect of defect concentration. Therefore, the following equation can be derived:

$$\kappa = \frac{1}{A + BT + Cx} \quad (3)$$

where, x is the concentration of defect and C describes the thermal resistance on conductivity by phonon-defect scattering in the defected system.

The parameters A and B are calculated by fitting thermal conductivity of pure ThO_2 as a function of temperature. To obtain parameter C, A and B are kept fixed and temperature dependent conductivity for each defect types is fitted according to Equation (3).

3.2. Callaway model

Thermal conductivity is analyzed using Callaway model [42], which assumes a Debye phonon spectrum. In this model, temperature dependence of κ is expressed in terms of sound velocity (v), phonon relaxation time (τ_p) and phonon frequency (ω):

$$\kappa = \frac{k_B}{2\pi^2 v}\left(\frac{k_B T}{\hbar}\right)^3 \int_0^{\Theta_D/T} \frac{\tau_P x^4 e^x}{(e^x - 1)^2}\, dx \quad (4)$$

where, $x = \hbar\omega/k_BT$. In Equation (4),ħ, Θ_D, and k_B denote the reduced Planck constant, the Debye temperature and the Boltzmann constant, respectively. The mean velocity of sound for ThO_2 is calculated to be 2129 ms^{-1} [43] using $v = k_B\Theta_D/\hbar\sqrt[3]{6\pi^2 n}$, where n is the number of atoms per unit volume and $\Theta_D = 259$ K [44]. The scattering mechanisms for thermal transport behavior affect the relaxation time. In ThO_2, this generally takes account of point defect scattering (D), boundary scattering (B) and Umklapp processes (U) according to Matthiessen's relaxation rule: $\tau_P^{-1} = \tau_D^{-1} + \tau_B^{-1} + \tau_U^{-1}$. The individual contributions from each term are as follows:

$$\tau_D^{-1} = D\,x^4T^4 = D\left(\frac{\hbar\omega}{k_B}\right)^4 \quad (5)$$

$$\tau_B^{-1} = B \quad (6)$$

$$\tau_U^{-1} = UT^3x^4e^{-\Theta_D/bT} = UT\left(\frac{\hbar\omega}{k_B}\right)^2 e^{-\Theta_D/bT} \quad (7)$$

The scattering constants: defect (D), boundary (B) and Umklapp (U, b) can be determined by fitting through thermal conductivity data. Using experimental results, Gofryk et al. [43] calculated these parameters for ThO_2 as reported in Table 1.

In this study, MD derived thermal conductivity of ThO_2 is fitted to Callaway model to determine the model parameters. For fitting purpose, at first pure ThO_2 is used and all the scattering constants are determined. In order to examine the effect of fission product and vacancy, only the defect scattering (D) term is refitted to MD data of defective ThO_2 system, where the terms for boundary scattering (B) and Umklapp process (U, b) are retained from that of pure system. Subsequently, D' for the defect species are calculated from the linear relationship of D and defect concentration, x:

$$D = D_{pure} + D'x \quad (8)$$

4. Results and discussion

4.1. Lattice parameter

The lattice parameter (L) measured for pure and defected $ThO_2$is shown in Fig. 1 as a function of temperature. L of ThO_2 with FPs and vacancy is reported in Fig. 1a and b respectively. The data in Fig. 1b is obtained from our previous MD study [21]. A linear increase with temperature is observed in both pure and defected systems. In Fig. 1b, for pure ThO_2, comparison with experimental studies [45,46] shows a good agreement with our MD derived values. Fig. 1a demonstrates that, despite showing similar rate of increase of L with temperature, the ThO_2-Xe system has larger lattice parameters than ThO_2-Kr system, which can be attributed to the bigger atomic radius of Xe. In addition, the vacancy also exhibits analogous rate of change of lattice parameter with temperature as compared to that by FPs. However, the increase in lattice parameter in defected ThO_2 due to FPs is much higher than that of vacancy. The level of defect concentration does not affect the temperature dependent variation of Lin all cases.

4.2. Enthalpy increment

In addition to change in the lattice parameter, the incorporation of FPs and porosities also lead to a change in the enthalpy of the system. In Fig. 2, the increment in enthalpy with respect to a standard condition (300 K) as a function of temperature, H(T)-H(300 K), is shown for pure thoria and defective ThO_2 with different concentration of Xe, Kr (Fig. 2a) and vacancy (Fig. 2b). The enthalpy increment increases linearly for both pure and defected system. For pure ThO_2, our results are in agreement with the reported values by Cooper et al. [16]. For clarity the relative change in enthalpy increment compared to pure thoria is calculated and shown for defective ThO_2 with Xe, Kr (Fig. 3a) and vacancy (Fig. 3b).

Fig. 3a exhibits that the relative change in enthalpy increment is marginally larger for the higher concentration of FP defects and the largest change is 1.3%. In general, the change is relatively smaller at

Table 1
The parameters of Callaway model for ThO_2, listed from Gofryk et al. [43] that are fitted to experimental thermal conductivity.

Boundary, Defect and Umklapp terms			
B (s^{-1})	D ($K^{-4}s^{-1}$)	U ($K^{-3}s^{-1}$)	b
2.663×10^8	72.31613	34816.892	2.2902802

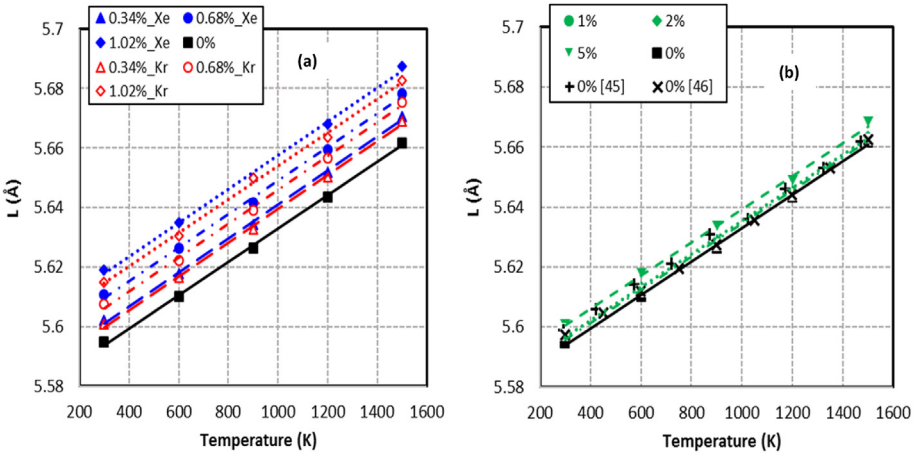

Fig. 1. Lattice parameter as a function of temperature for pure and defective ThO_2 with different percentage of (a) Xe and Kr, (b) vacancy [21]. The lines represent the best linear fit. The experimental studies are by Mathews et al. [45] and Yamashita et al. [46].

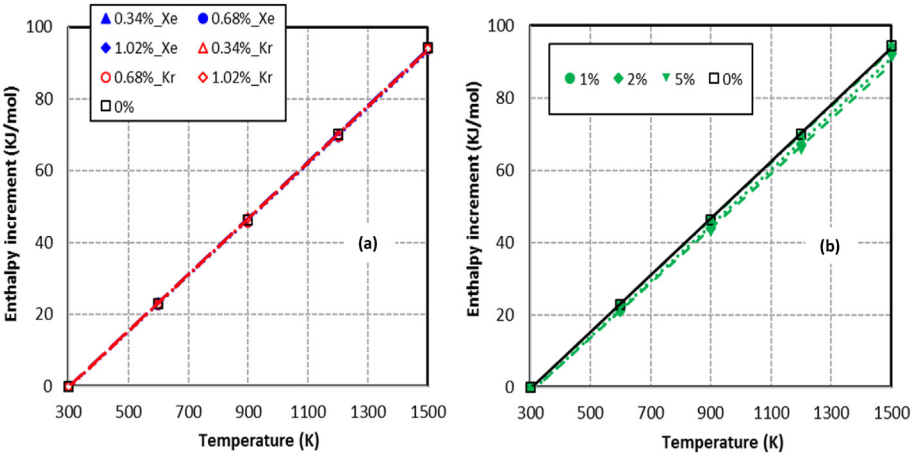

Fig. 2. Enthalpy increment (with respect to the enthalpy of 300 K) as a function of temperature for pure and defective ThO_2 with different percentage of (a) Xe and Kr, (b) vacancy. The lines represent the best linear fit.

higher temperature. This trend is obvious for higher concentration of vacancies (Fig. 3b). In particular, for 2% and 5% vacancy, a change of ~6% is observed between 600 K and 1500 K temperature. However, for 1% vacancy, the maximum difference is 0.7%, which is noticeably lower than that of FPs for the similar concentration of Xe and Kr.

4.3. Specific heat

In nuclear operation, since temperature can increases significantly within the fuel material, it is of significant interest to measure the specific heat and its dependence on fission generated defects. The specific heat at constant pressure is calculated from the first derivative of the enthalpy increment with respect to temperature using the following relation:

$$c_p = \frac{1}{n}\left(\frac{\partial H}{\partial T}\right)_P \tag{9}$$

where, n is the number of moles and $\left(\frac{\partial H}{\partial T}\right)_P$ is obtained from the slope of the plot of enthalpy increment as a function of temperature. The slope is extracted by fitting a straight line to the enthalpy changes at a specific temperature and other data points within 50 K on either side.

The calculated specific heat as function of temperature for pure ThO_2 is shown in Fig. 4. Our measured c_p values agree well with that of Cooper et al. [16]. For comparison, c_p from experiments are included in the figure. In general, the specific heat of ThO_2 increases with temperature. Fig. 4 indicates that the calculated values reasonably agree with the counterpart of experiments at higher

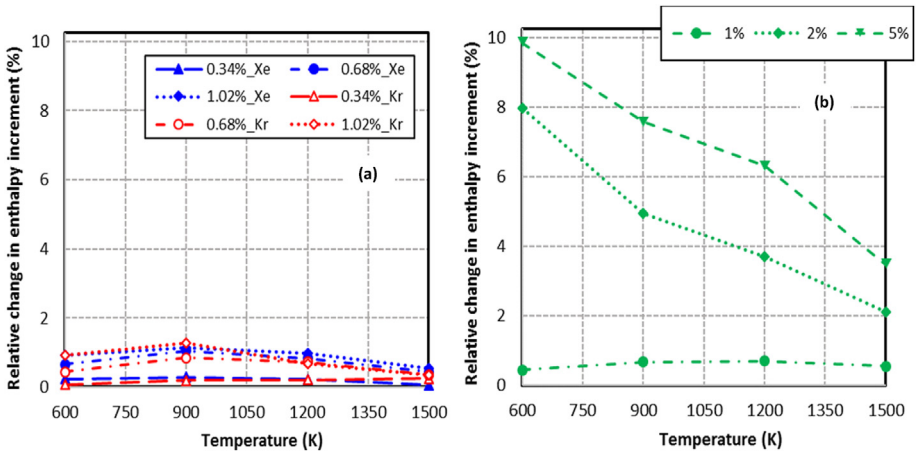

Fig. 3. Relative change in enthalpy increment of defective ThO_2 compared to pure ThO_2as a function of temperature for different concentration of (a) Xe and Kr, (b) vacancy.

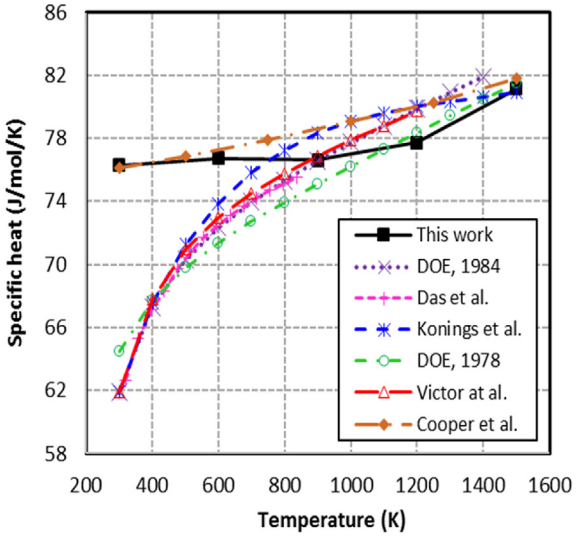

Fig. 4. Specific heat (with respect to the enthalpy of 300 K) for pureThO_2compared with experimental measurements of DOE-1984 [49], Das et al. [50], Konings et al. [51], DOE-1978 [52], Victor et al. [53] and Cooper et al. [16].

temperature. However, MD derived c_p shows a noticeable overestimation compared to the experimental results in the low temperature regime. It has been previously reported that the empirical interatomic potentials typically overvalue the specific heat at lower temperature [47,48]. This discrepancy is mainly due to the absence of mean electronic effect in classical MD approach at these temperatures. In addition, the quantum mechanical features, which is also absent in MD models, can play a considerable role. Furthermore, the overestimation of MD values can also be attributed to the possible presence of crystal defects, such as dislocations and grain boundaries, in the experimental observations, not accounted by the simulations.

The effect of Xe and Kr (Fig. 5a) and fuel vacancy (Fig. 5b) on specific heat of ThO_2 as a function of temperature are shown in Fig. 5. The general trend of temperature dependence of c_p in defective systems are similar to those in pure oxide. As reported in Fig. 5a, MD derived c_p values for 0.34% Xe and Kr are similar to that of pure ThO_2 at all studied temperature. For higher concentration of FP, in both ThO_2-Xe and ThO_2-Kr systems, the specific heat values are somewhat lower than the counterpart of pure system. Considering all temperatures, for 1.02% Xe and Kr, the reduction in c_p is 0.9–1.8% and 0.4–1.7% respectively.

In Fig. 5b, the effect of vacancy on specific heat is shown, where the change in c_p as a function temperature is analogues to that of FPs. At 300 K, 1%, 2% and 5% vacancy lead to only 0.8%, 2.4% and 4.7% reduction respectively in c_p. In contrast, at higher temperatures, there is no noticeable difference in c_p between pure and defected system for any level of vacancy concentration. Therefore, our MD derived c_p values of thoria with FPs and vacancy indicate that, for smaller concentration ($\leq$1.02%), the reduction in specific heat is insignificant. However, for higher concentration (~5%), the defected systems show considerable difference compared to the pure system mainly at low temperature within the investigated range.

4.4. Thermal conductivity of pure ThO_2

Using Muller-Plathe approach [41], thermal conductivity is measured from a constant gradient in temperature profile between the edge and center bin of the supercell. Fig. 6a shows steady state temperature distribution along heat transfer direction of in pure thoria for the largest system ($5 \times 5 \times 200$ unit cells) at all studied temperatures. The figure demonstrates higher temperature at the center bin (hot) and lower at the edge bin (cold). The slope of the steady state profile determines the temperature gradient. Higher slope at elevated temperature indicates that the magnitude of the gradient increases with the increase in temperature.

In Fig. 6b, the variation in $1/\kappa$ as a function of $1/L_z$ is shown for pure ThO_2 at all temperatures. L_z denotes the lengths of 5 supercells with different sizes. The effect of system size demonstrates that the shorter supercells underestimate the thermal conductivity. In MD approach, due to finite size of the simulation box, the mean free path of the phonons are limited, which increases the phonon scattering between the center and edge bins in the system. Therefore, MD calculation results in lower thermal conductivity, particularly more for shorter systems and κ increases with the increase in cell size. The fitted lines in Fig. 6b indicate a linear relationship of conductivity with supercell length at all temperatures. Bulk thermal conductivity that represents infinitely large system is calculated by extrapolating the linear trend to infinite length, as shown in Fig. 6b [15,20]. Y-intercept of the fitted lines is used to determine the bulk κ. This technique has been repeated for ThO_2-Xe, ThO_2-Kr and ThO_2–vacancy systems. Bulk values of thermal conductivity has been used in all cases for the rest of this paper.

The calculated bulk thermal conductivity of pure ThO_2 is shown in Fig. 7 as a function of temperature (300–1500 K). The uncertainties are calculated from the deviation of the linear fit (see

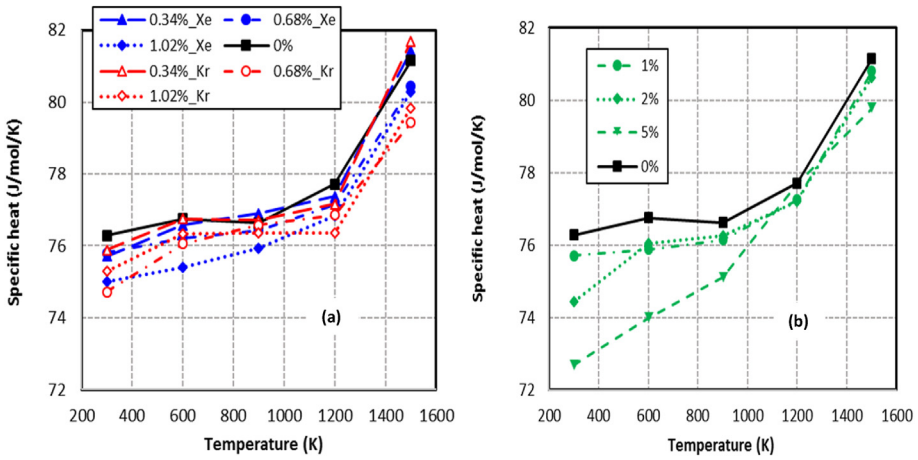

Fig. 5. Specific heat (with respect to the enthalpy of 300 K) as a function of temperature for pure and defective ThO_2 with different concentration of (a) Xe and Kr, (b) vacancy.

Fig. 6b). For comparison, relevant experimental studies [54–58] are also included. MD results show a gradual reduction in κ with the increase in temperature, which is analogous to experimental observation. At elevated temperature, higher thermal vibration induces more scattering in the phonons that limits thermal transport and reduces thermal conductivity [59]. Fig. 7 demonstrates that the experimentally determined thermal conductivity is lower as compared to the counterpart measured from MD simulations, in particular at low temperature. This discrepancy is also observed in the previous investigations [15,29]. In real materials, the impurities, even in trace amount, can impede thermal transfer behavior considerably and in turn reduces the conductivity. However, in MD approach, no such defect is present in the structure. The current work investigates the effect of some fission-generated defects on MD derived thermal conductivity. Fig. 7 also indicates that the discrepancy between the calculated and experimental results is large at low temperature and vice versa. The classical MD simulations cannot accurately measure κ in the low temperature region, where average electronic effect or quantum mechanics tend to control thermal transport behavior [29]. However, these features are not included in MD approach [47,48], which can be attributed to the larger discrepancy between MD and experimental results at lower temperature.

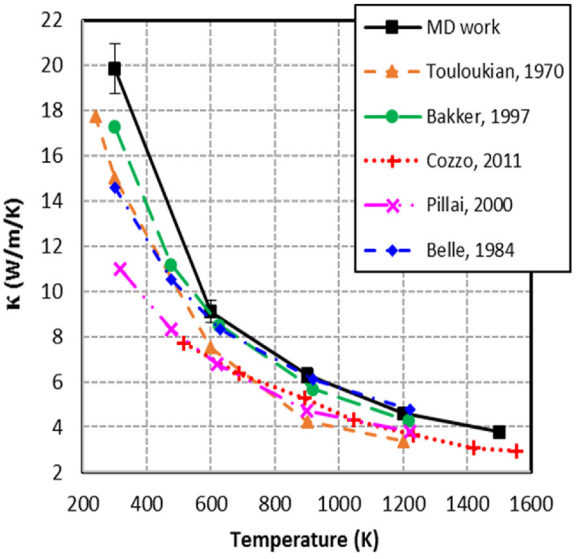

Fig. 7. Comparison of MD derived bulk thermal conductivity of pure ThO_2as a function of temperature with experimental studies of Touloukian et al. [54], Bakker et al. [55], Cozzo et al. [56], Pillai et al. [57] and Belle et al. [58].

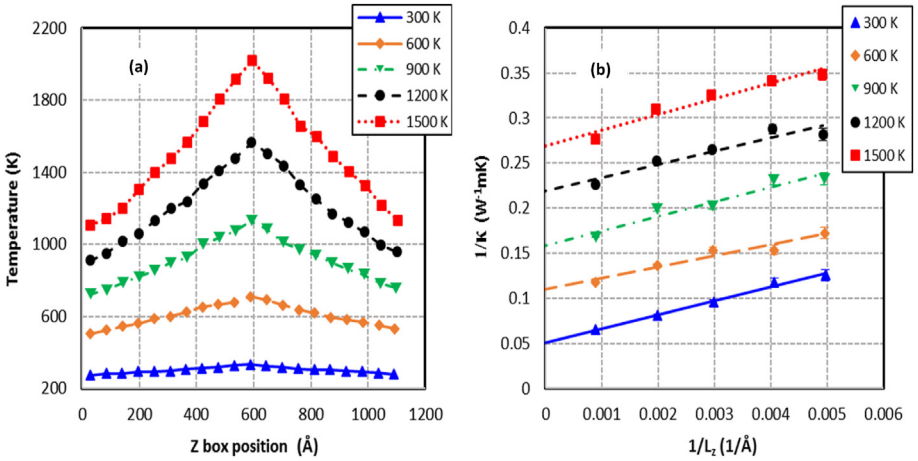

Fig. 6. In pure ThO_2 and for all studied temperatures (a) Steady state temperature profiles for the largest system (5 × 5 × 200 unit cells), (b) Inverse of thermal conductivity as a function of inverse of supercell length.

4.5. Thermal conductivity of ThO_2-vacancy and ThO_2-Xe,Kr systems

Fig. 8a and b respectively illustrate the effect of fission products and vacancy on the thermal conductivity of defected ThO_2 as a function of temperature for all studied concentrations of defects. Both the FPs and vacancies significantly reduce κ in thoria, particularly at low temperatures. The defects incorporate non-uniform cation and anion sublattice in the structure. It has been reported that the scattering associated with non-uniform cation sublattice reduces the phonon mean free path in actinide oxides [15]. Therefore, substitutional addition of the defects in ThO_2 can lead to enhanced phonon scattering due to reduction in mean free path and result in lower thermal conductivity in the defected system. The reduction in κ by FP and vacancy largely depends on the temperature. Fig. 8 demonstrates that, for any specific concentration, the difference in conductivity between pure and imperfect ThO_2 decreases with the increase in temperature. At elevated temperature, the non-uniform sublattice induced phonon scattering is limited due to high thermal vibration. The estimated impact of defects on thermal conductivity in ThO_2 is qualitatively analogous to the counterpart in UO_2, observed by Liu et al. [29].

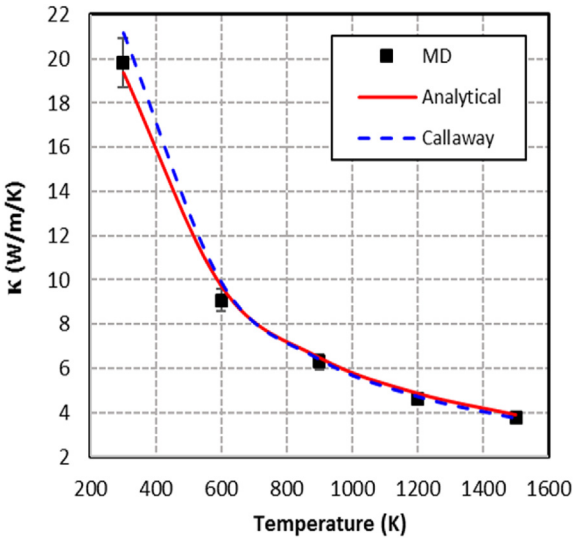

Fig. 9. Thermal conductivity of pure ThO_2 vs. temperature derived from MD simulation, by fitting Callaway and Analytical model.

4.6. The models of thermal conductivity

4.6.1. For pure ThO_2

The fitted Callaway and Analytical model along with the MD derived thermal conductivity of pure ThO_2as a function of temperature are shown in Fig. 9. The fitting parameters for both models are reported in Table 2. In general, a good agreement is observed between these models and the MD data. However, in the low temperature region, there may exist marginal discrepancy. Since mean electronic or quantum effects tend to dominate at low T, which is absent in classical MD approaches, these simulations cannot precisely determine thermal conductivity in that temperature regime. This is related to the inconsistencies in low-temperature specific heat between our calculated results and the experimental values as reported in Fig. 3.

In Table 2, for pure ThO_2, the Callaway model parameters *B*, *D*, *U*, *b* and Analytical model parameters *A*, *B* are listed. It can be noticed that, for Callaway model, the magnitudes of MD derived terms are very close to the experimental counterparts (see Table 1). In comparison to UO_2 [29], the terms for defect scattering (*D*) and Umklapp process (*U*) are lower for ThO_2 by 2.2and 1.2 times respectively. This may indicate that the scattering in thermal transportation is relatively less probable in ThO_2 compared to that in UO_2. In Analytical model, the terms *A* and *B* represents the strength of the temperature dependent behavior of thermal conductivity. The parameter *B* for ThO_2 is 1.2 times lower compared to that for UO_2 [29]. Since UO_2 is magnetic, the term *A* may contain the contribution from some additional factors related to magnetic spin scattering process.

4.6.2. Defect scattering by analytical model

The values of *C* for the systems with all types of defect are listed in Table 3. The fitted Analytical model for the defective ThO_2 systems is shown Fig. 10.For all defects, the model shows a good fit with the MD derived thermal conductivity. The data in Table 3 demonstrate that the thermal resistance to conductivity by FPs is significantly higher than that of vacancy. In addition, generally *C* values are larger for ThO_2-Xe systems compared to that of ThO_2-Kr systems. This indicates that the rate of reduction in conductivity for Xe atoms is relatively greater than the counterparts of Kr atoms. Further relevant evidence is reported in Section 4.7.

For comparison with UO_2, Liu et al. [29] reported that, with Cooper potential [36],the *C* parameter for U-vacancy is 32.74 W^{-1}mK and, with Busker potential [60], the *C* values for U- and O-vacancy are 23.78 and 12.74 W^{-1}mK respectively. These

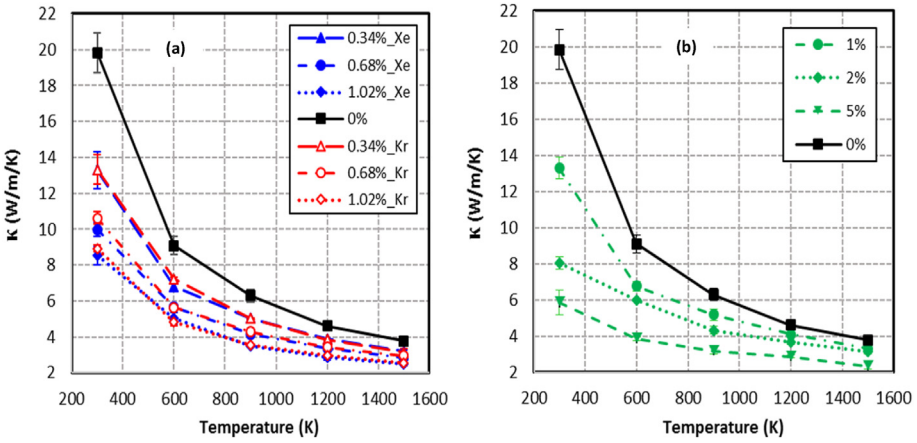

Fig. 8. Bulk thermal conductivity as a function of temperature for pure ThO_2 and different concentration of (a) Xe and Kr, (b) vacancy.

Table 2
MD derived parameters of the Callaway and Analytical model for pure ThO_2.

Callaway model			
B (s^{-1})	D ($K^{-4}s^{-1}$)	U ($K^{-3}s^{-1}$)	b
2.66178×10^{8}	71.7935	33402.7	2.25584
Analytical model			
A ($W^{-1}mK$)		B ($W^{-1}m$)	
27.464×10^{-14}		17.1833×10^{-5}	

Table 3
The values of C (Analytical model) and $D^{'}$ (Callaway model) for ThO_2 systems with Xe, Kr and vacancy are listed.

System	Analytical model, C ($W^{-1}mK$)	Callaway model, $\boldsymbol{D}^{'}$ ($K^{-4}s^{-1}$)
ThO_2-Xe	7.81 ± 0.27	126475.0 ± 5580.56
ThO_2-Kr	7.30 ± 0.22	112259.3 ± 2879.47
ThO_2-vacancy	2.95 ± 0.53	42265.04 ± 3609.12

values are much higher than that for vacancies in ThO_2. For Urania, as described in Ref. [29], Busker potential [60] predicts the C terms to be 33.9 $W^{-1}mK$ for Xe, which is also larger than counterparts in ThO_2. Therefore, our results indicate that the resistance to thermal conduction, as represented by C parameter in Analytical model, is larger in UO_2 compared to ThO_2. It is to be noted that the spin scattering effect has been incorporated in Urania since it is magnetic and this can be attributed to the difference in the results of UO_2 and ThO_2.

4.6.3. Defect scattering by callaway model

The defect scattering by Callaway model for the defective ThO_2 systems is shown in Fig. 11. A reasonable agreement is observed between MD results and the fitted model for all defects and concentrations. The $D^{'}$ parameter, calculated using Equation (8), is reported in Table 3. The data exhibits that the scattering by defect is noticeably higher for the FPs compared to the counterpart of vacancy. In FPs, $D^{'}$ values for Xe is somewhat larger than that of Kr. The behavior of $D^{'}$ term in Callaway model is similar to that of C term of Analytical modeling for both ThO_2-FPs and ThO_2-vacancy systems. For UO_2, it has been reported that the $D^{'}$ parameter for Xe is higher than those for the other FPs [29,61] by a considerable amount and therefore Xe largely dominates the degradation of thermal conductivity in nuclear fuel.

As reported by Liu et al. [29], in UO_2, Busker potential derives $D^{'}$ to be 235,000 $K^{-4}s^{-1}$ for Xe, which is higher than our calculated $D^{'}$ values for Xe in ThO_2. In addition, Ref. [29] states that Cooper potential [36] determined $D^{'}$ for U-vacancy is 172,000 $K^{-4}s^{-1}$and Busker potential [54] measured $D^{'}$ forU- and O-vacancy is 172,000 and 79,400 $K^{-4}s^{-1}$ respectively. According to Table 3, these values for UO_2 are much higher than that of ThO_2. All the $D^{'}$ values for defective UO_2 is corrected for spin scattering to take into account the magnetic effect. The magnetic scattering may lead to higher degradation of thermal conductivity, as evidenced by defect scattering term ($D^{'}$) in Callaway model, in UO_2 in comparison to ThO_2.

4.7. The reduction of κ by fission products and vacancies

The quantitative measurement of the reduction in thermal conductivity of ThO_2 by fission product and vacancy as function of defect concentration is respectively reported in Fig. 12a and b for all temperatures. The percentage of reduction is calculated using the following expression:

$$Reduction\ (\%) = (\kappa_P - \kappa) / \kappa_P * 100$$

where, κ_P and κ representthermal conductivity of pure and defected ThO_2. Fig. 12 shows an increase in the reduction of conductivity with the increase in defect concentration for all temperatures.

It is demonstrated in Fig. 12 that, for any specific defect concentration, the degree of reduction in thermal conductivity decreases with the increase in temperature. For the largest concentration of defects, the percentage of reduction in κ decreases from 300 to 1500 K by nearly ~23% and ~32% for FPs and vacancies respectively. Nevertheless, for the lowest concentration, the decrease in reduction is smaller, roughly 17% for FPs and 20% for vacancies. Fig. 12 also indicates that the rate of reduction in κ with

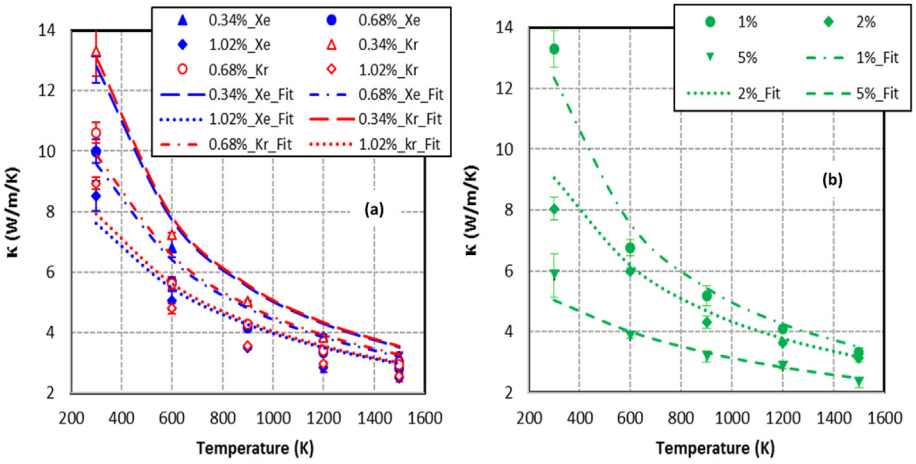

Fig. 10. Thermal conductivity of defective ThO_2 as a function of temperature derived by fitting Analytical model for different concentration of (a) Xe and Kr, (b) vacancy.

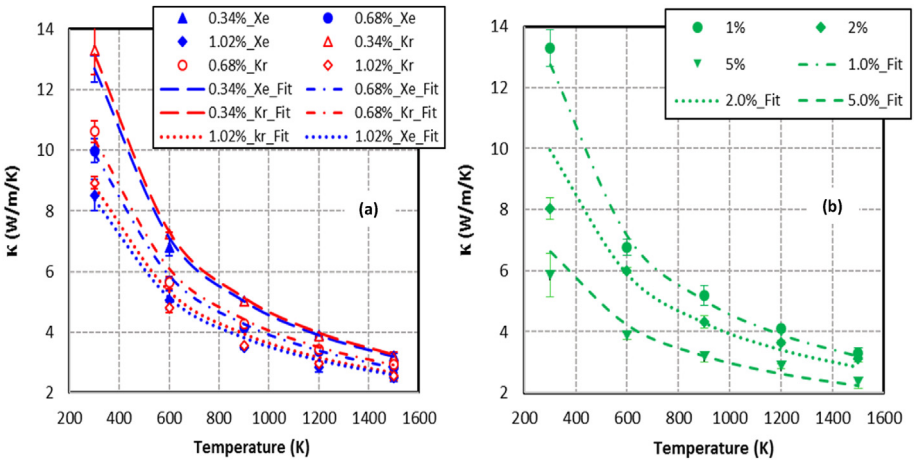

Fig. 11. Thermal conductivity of defective ThO_2 as a function of temperature derived by fitting Callaway model for different concentration of (a) Xe and Kr, (b) vacancy.

respect to the concentration of FP or vacancy is comparatively higher for the systems with lower defect concentration. As shown in Fig. 12a, at 300 K for 1.02%Xe, nearly 57% reduction is reported, however 33% of that decrease is noticed at 0.34%Xe. Similarly, Fig. 12b illustrates that, at 300 K, 33% and 70% reduction in κ is observed for 1% and 5% vacancy respectively.

In addition, Fig. 12a and b quantitatively illustrate a comparison between the effect of FPs and vacancy. FPs exerts stronger influence on the reduction of thermal conductivity compared to that by vacancies at all temperatures. In addition, the reduction in ThO_2-Kr is marginally smaller than in ThO_2-Xe, which is evident for higher concentration of defects. Similar trend of FPs is observed for the elastic properties in ThO_2 [21]. The atomic radius of Xe and Kr is close to that of Th^{4+} and O^{2-} ions respectively, while Xe atoms are larger than Kr atoms. Therefore, it is possible that somewhat stronger strain field will arise at the sub-lattices in ThO_2-Xe systems in comparison to ThO_2-Kr. As reported in Fig. 1, the lattice parameter of ThO_2-FPs is much larger than that of ThO_2-vacancy. This can cause more phonon scattering and lead to comparatively higher degradation in thermal conductivity for ThO_2 with FPs compared to vacancy. In particular, in the case of 1% defect, the reduction of conductivity by Xe is higher compared to counterpart for vacancy by ~24% at 300 K and ~21% at 1500 K. For the same defect concentration, the reduction rate for Xe is higher than that of Kr by 2% at 300 K and 0.5% at 1500 K.

The calculated degree of reduction in κ for $ThO_2$is compared with that of UO_2 and is shown in Fig. 13 as a function of temperature. In particular, Fig. 13 illustrates the comparison between ThO_2-1.02%Xe and UO_2-1.03%Xe [29]. The degradation of conductivity by FPs is higher in UO_2 compared to that in ThO_2 and the difference varies from 13% to 29% within studied temperature range. In addition to magnetic effect (spin scattering), as discussed in Section 4.6.2 and 4.6.3, the lattice parameter (L) can also play a role in determining the resistance to thermal conduction in defective UO_2 and ThO_2. Due to non-uniform cation and anion sub-lattice in the imperfect systems, a lattice disorder exists in the structure. Cooper et al. [15] reports that, in actinide oxides, smaller disorder generates lower strain field around the substitutional defects. Since L of UO_2 is smaller than that of ThO_2, the insertion of FPs can exert higher strain in the sub-lattice of UO_2 and therefore cause higher reduction in conductivity.

4.8. *Effect of distribution of defects on κ*

In order to investigate the effect of defect distribution on thermal transport, besides addition of individual FP and vacancy at different lattice positions, the defect atoms have also been inserted in close proximity to each other at the Schottky-vacancy sites in the form of cluster. In particular, defect clusters with 6, 12, 18 and 24 atoms for 1.02% of Xe and 1% vacancy at 300 K has been studied.

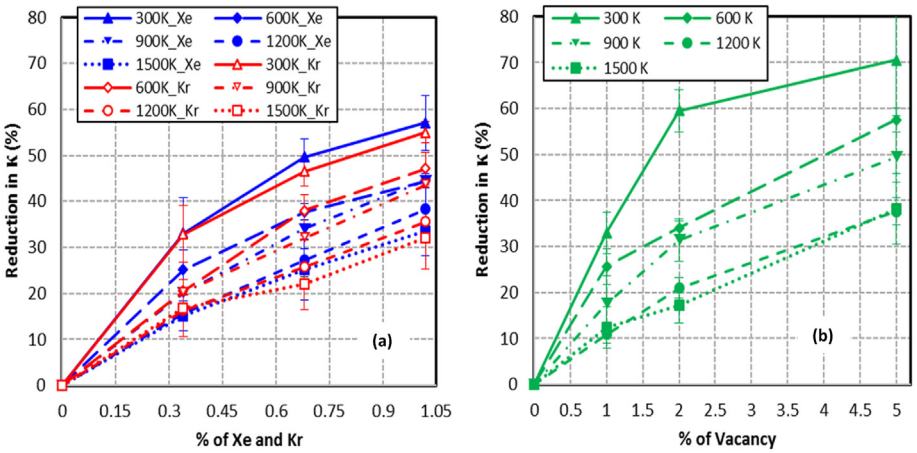

Fig. 12. Reduction in bulk thermal conductivity of defective ThO_2 as a function of concentration of (a) Xe and Kr, (b) vacancy for all studied temperatures.

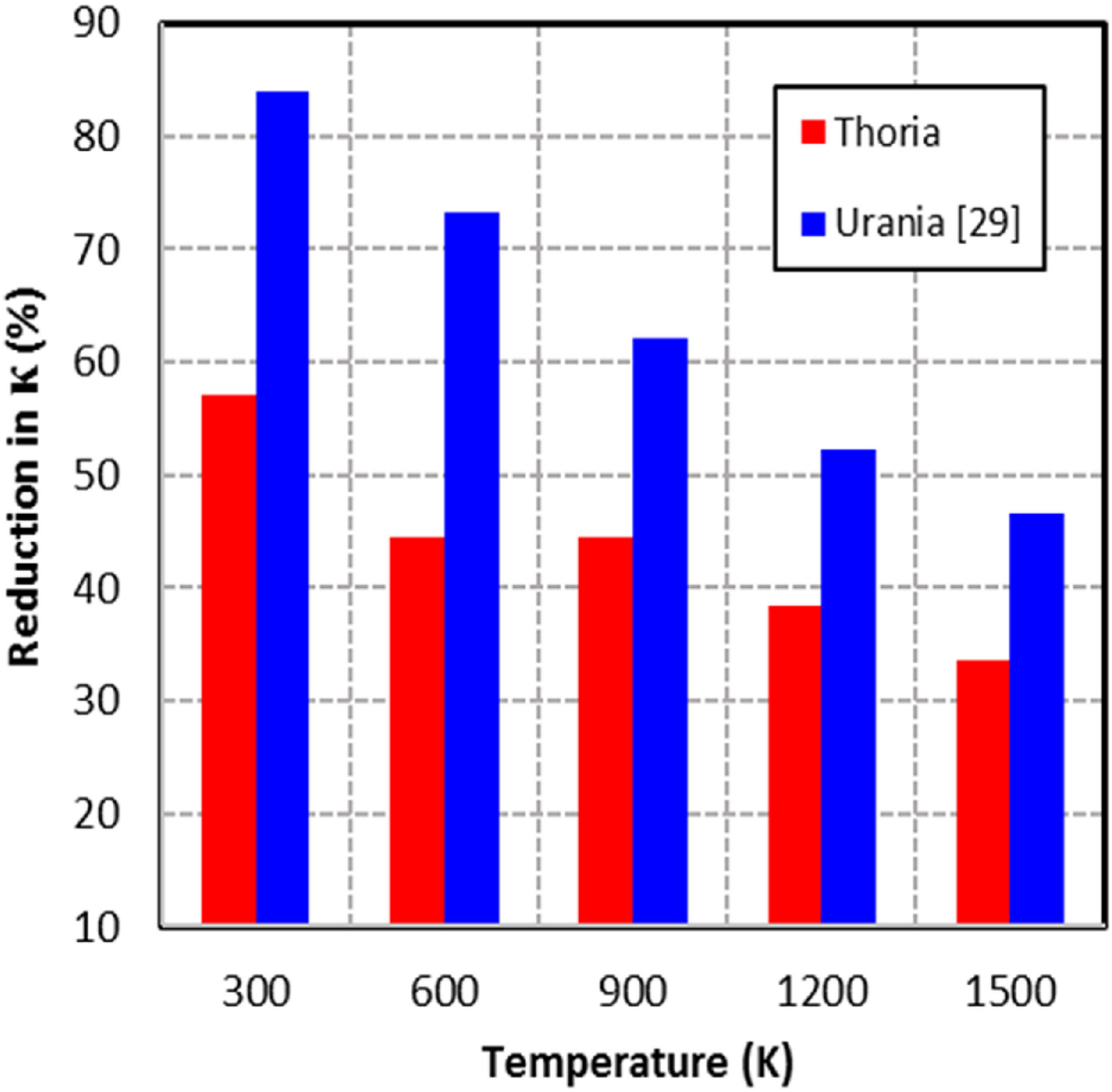

Fig. 13. Comparison of reduction in bulk thermal conductivity between (a) ThO_2-1.02%Xe and UO_2-1.03%Xe [29] as a function of temperature.

Fig. 14a, b and 14c show the representative snapshots of defect clusters with 6, 12 and 24 atoms respectively. For clarity, only Xe atoms are shown. As illustrated in the figures, the defects are distributed along the direction of heat transfer (z-axis).

The change in energy of the systems as a function of cluster size (number of atoms per cluster) of the defects for Xe and vacancy are shown in Fig. 15a and b respectively. The figures demonstrate a negligible amount of variation in the energy with the change in cluster size. The maximum change in energy between the clusters of studied size is found to be 0.1 and 0.05% for Xe and vacancy, respectively. Therefore, it can be reported that, during fission event in nuclear operation, the formation of defect clusters with different size is equally probable. However, it would be of great interest to examine how does the clustering of defects impact the thermal transport behavior in ThO_2.

Fig. 16 demonstrates the change in bulk thermal conductivity as a function of the size of defect clusters. ThO_2 with 1.02% Xe and 1% vacancy is represented in Fig. 16a and b separately. The increase in number of atoms in the clusters leads to significant decrease in conductivity and the reduction is almost linear. The effect of cluster size is stronger in ThO_2-vacancy system in comparison to that in ThO_2-Xe. At 300 K, for Xe and vacancy, the 24-atom cluster decreases κ by 53% and 30% respectively. In addition, the linear fit determines that the rate of degradation in thermal conductivity is

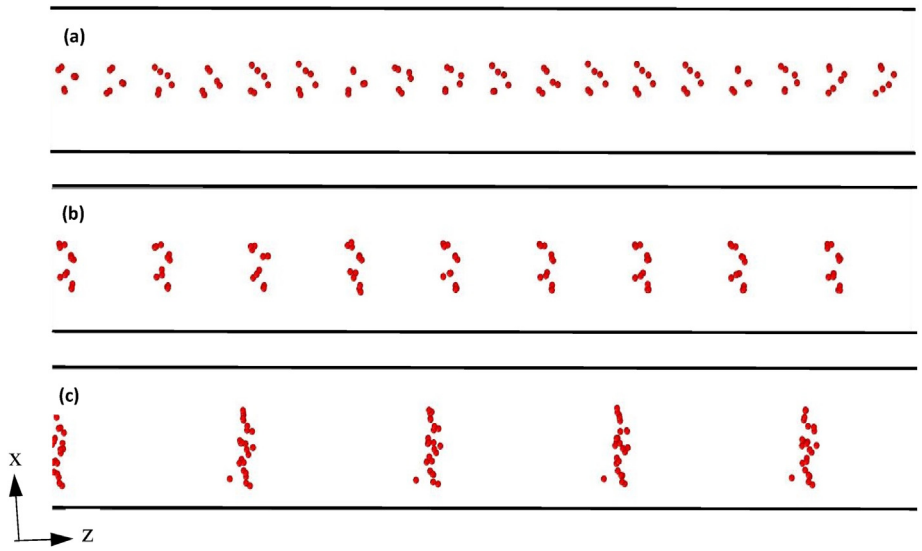

Fig. 14. Distribution of Xe atoms showing the clustering of (a) 6 atoms, (b) 12 atoms and (24 toms) in 1.02% Xe system at 300 K. For clarity, only the Xe atoms are shown.

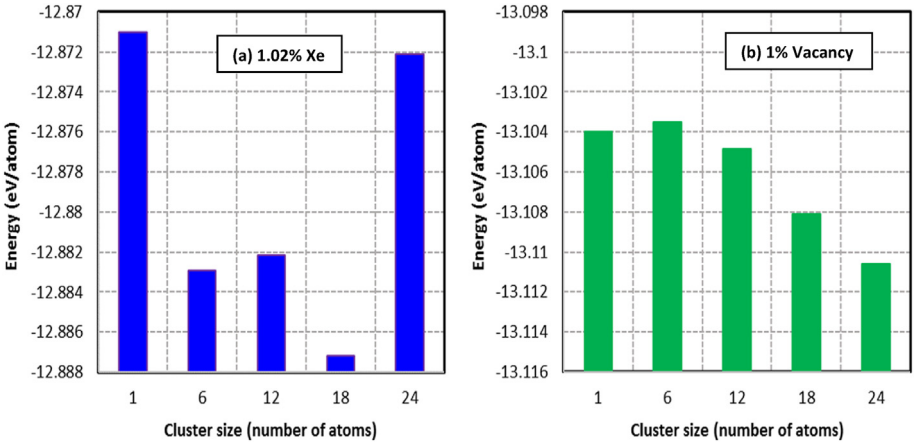

Fig. 15. Variation in the energy with cluster size (number of atoms) in (a) 1.02% Xe and (b) 1% vacancy system at 300 K.

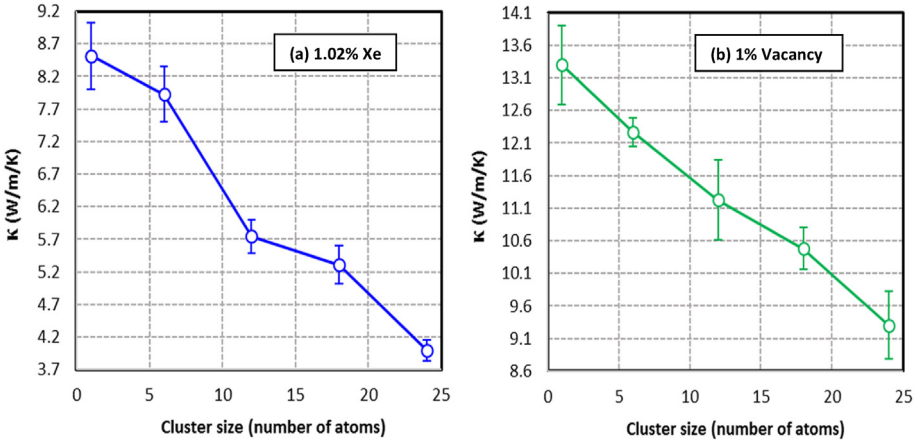

Fig. 16. Variation in bulk thermal conductivity with the cluster size (number of atoms) in (a) 1.02% Xe and (b) 1% vacancy system at 300 K.

0.2 and 0.17 W/m/K per atom (cluster size) for Xe and vacancy. Therefore, we report that the degree of reduction in thermal conductivity with the increase in cluster size is higher for the FPs compared to that for the vacancy.

5. Conclusion

In this MD study, we investigate the effect of two typical FPs (Xe, Kr) and vacancy on mainly thermal conductivity along with other thermo-physical properties, such as specific heat (c_p)and enthalpy increment, in ThO_2within the range of 300−1500 K temperature. Our studied defect concentrations are 0.34%, 0.68%, 1.02% for FPs and 1%, 2%, 5% for vacancies. Our calculated low-temperature c_p shows a significant overestimation compared to experimental values. This is typically observed in the previous studies and attributed to the absence of quantum effects in MD approach. However, nonexistence of mean electronic contribution in MD simulations can also affect thermal transportation at the low temperature regime. We observe that the FPs and vacancies, with smaller concentration ($\leq$1.02%), do not have noticeable effect on specific heat at all temperature. For ~1% defect content, a maximum reduction of 1.8%, 1.7% and 1.1% is obtained in ThO_2-Xe and ThO_2-Kr and ThO_2-vacancy systems respectively. In contrast, for higher defect concentration in ThO_2-vacancy, for the reduction in c_p is considerable at low temperatures, which however becomes negligible at elevated temperature. In case of The relative change in enthalpy increment in defected ThO_2 with lower concentration ($\leq$1.02%) compared to pure system is small at all temperatures. For higher defect concentration ($\geq$2%) in ThO_2-vacancy, the change in enthalpy increment decreases with temperature.

MD derived thermal conductivity for pure ThO_2 as a function of temperature shows a reasonable agreement with the relevant experimental data. We observe that the FPs and vacancy significantly reduce thermal conductivity in ThO_2. The reduction in κ decreases with the increase in temperature. The change in conductivity with temperature for both pure and defected system is described using a Callaway and Analytical model. The scattering parameters, calculated from these models, for each fission product and vacancy in ThO_2 are compared with those of UO_2. In particular, the quantitative phonon and defect scattering terms in Analytical model are essential to develop fuel performance model.

Our results predict that the percentage of reduction (R) in thermal conductivity of ThO_2 by the defects follows the trend $R_{FP} > R_{Vacancy}$. Within the studied concentrations of FPs, R_{Xe} is found to be marginally higher than R_{Kr}. In addition, it has been observed that the rate of reduction in κ with respect to defect content is relatively higher for the systems with lower FP or vacancy concentration. Comparison with UO_2 depicts that the percentage of degradation in thermal conductivity by the similar type and concentration of defects is lower in ThO_2.

Besides individual defect, the impact of defect clusters with 6, 12, 18 and 24 atoms for 1.02% Xe and 1% vacancy at 300 K has also been studied in this work. Negligible amount of change in energy as a function of number of atoms per cluster predicts that the probability of defect cluster formation with different size is equal during fission event in nuclear operation. We report that conductivity decreases almost linearly with the increase in cluster size. The rate of reduction with cluster size is higher in ThO_2-Xe system than the counterpart in ThO_2-vacancy system.

Characterization of fuel performance in nuclear operation is largely controlled by the thermal conductivity and its dependence on radiation generated defects. However, to date, no work has been focused on the effect of FPs and vacancies on conductivity in ThO_2. Therefore, our MD results can assist in understanding and predicting the thermal transport behavior in fission event.

Data availability

The raw/processed data required to reproduce these findings cannot be shared at this time as the data also forms part of an ongoing study.

Declaration of competing interest

No conflict of interest.

CRediT authorship contribution statement

M.J. Rahman: Conceptualization, Investigation, Methodology, Software, Data curation, Formal analysis, Visualization, Validation, Writing - original draft, Writing - review & editing, Project administration. **B. Szpunar:** Conceptualization, Resources, Supervision, Writing - review & editing, Project administration. **J.A. Szpunar:** Conceptualization, Resources, Supervision, Writing - review & editing, Funding acquisition, Project administration.

Acknowledgement

The authors would like to acknowledge Canadian Natural Sciences and Engineering Research Council (NSERC) for the financial support. We are also thankful to the high performance supercomputing facilities at Compute Canada and Plato from University of Saskatchewan.

References

[1] P.A. Jackson, J.A. Turnbull, R.J. White, International Atomic Energy Agency, Report No. IAEA-TECDOC-687, 1989.
[2] R.L. Williamson, J.D. Hales, S.R. Novascone, M.R. Tonks, D. Gaston, C.J. Permann, D. Andrs, R.C. Martineau, J. Nucl. Mater. 423 (2012) 149−163.
[3] C. Unal, B.J. Williams, A. Yacout, D.M. Higdon, Nucl. Eng. Des. 263 (2013) 102−128.
[4] M.W.D. Cooper, S.C. Middleburgh, R.W. Grimes, Prog. Nucl. Energy 72 (2014) 33−37.
[5] S.C. Middleburgh, R.W. Grimes, K.H. Desai, P.R. Blair, L. Hallstadius, K. Backman, P. Van Uffelen, J. Nucl. Mater. 427 (2012) 359−363.
[6] D. Olander, J. Nucl. Mater. 389 (2009) 1−22.
[7] http://www.thoriumpowercanada.com/technology/the-fuel/thorium-vs-uranium-fuels/.
[8] D.R. Lide, Handbook of Chemistry and Physics (86th Version), CRC Press Inc., 2005.
[9] Thorium Fuel Cycle: Potential Benefits and Challenges, International Atomic Energy Agency (IAEA) Technical Document, 2005 vol. 1450.
[10] J. Belle, R.M. Berman, Thorium Dioxide: Properties and Nuclear Application, U.S. DOE/NE-0060, Naval Reactors Office, Washington, DC, 1984.
[11] Y.S. Touloukian, in: R.W. Powell, C.Y. Ho, P.G. Klemens (Eds.), Thermal Conductivity: Nonmetallic Solids, *Thermophysical Properties of Matter*, vol. 2, IFI/Plenum, New York, 1970.
[12] K. Bakker, E.H.P. Cordfunke, R.J.M. Konings, R.P.C. Schram, J. Nucl. Mater. 250 (1997) 1−12.
[13] C. Cozzo, D. Staicu, J. Somers, A. Fernandez, R.J.M. Konings, J. Nucl. Mater. 416 (2011) 135−141.
[14] C.G.S. Pillai, P. Raj, J. Nucl. Mater. 277 (2000) 116−119.
[15] M.W.D. Cooper, S.C. Middleburgh, R.W. Grimes, J. Nucl. Mater. 466 (2015) 29−35.
[16] M.W.D. Cooper, S.T. Murphy, P.C.M. Fossati, M.J.D. Rushton, R.W. Grimes, Proc. Roy. Soc. A 470 (1−14) (2014) d.
[17] B. Szpunar, J.A. Szpunar, Ki-Seob Sim, J. Phys. Chem. Solid. 90 (2016) 114−120.
[18] B. Szpunar, J.A. Szpunar, Solid State Sci. 36 (2014) 35−40.
[19] Jiang-Jiang ma, Ji-Guang Du, Ming-Jie Wan, G. Jiang, J. Alloys Compd. 627 (2015) 476−482.
[20] M.J. Rahman, B. Szpunar, J.A. Szpunar, Mater. Res. Express 4 (1−8) (2017), 075512.
[21] M.J. Rahman, B. Szpunar, J.A. Szpunar, J. Nucl. Mater. 510 (2018) 19−26.
[22] M.W.D. Cooper, C.R. Stanek, X.-Y. Liu, D.A. Andersson, MRS Advances 1 (2016) 2483−2487.
[23] J. Park, E.B. Farfan, C. Enriquez, Nucl. Eng. Tech. 50 (2018) 731−737.
[24] I.C. Hobson, R. Taylor, J.B. Ainscough, J. Phys. D Appl. Phys. 7 (1974) 1003−1016.
[25] S. Ishimoto, M. Hirai, K. Ito, Y. Korei, J. Nucl. Sci. (Seoul) 31 (1994) 796−802.
[26] N. Kuganathan, P.S. Ghosh, C.O.T. Galvin, A.K. Arya, B.K. Dutta, G.K. Dey,

R.W. Grimes, J. Nucl. Mater. 485 (2017) 47–55.
[27] D. Yun, M. Stan, J. Mater. Res. 28 (2013) 2308–2315.
[28] M. Colbert, F. Ribeiro, G. Tréglia, J. Appl. Phys. 115 (1–10) (2014), 034902.
[29] X.-Y. Liu, M.W.D. Cooper, K.J. McClellan, J.C. Lashley, D.D. Byler, B.D.C. Bell, R.W. Grimes, C.R. Stanek, D.A. Andersson, Phys. Rev. Appl. 6 (1–19) (2016), 044015.
[30] J. Park, E.B. Farfán, K. Mitchell, A. Resnick, C. Enriquez, T. Yee, J. Nucl. Mater. 504 (2018) 198–205.
[31] L. Malakkal, A. Prashad, E. Jossou, J. Ranasinghe, B. Szpunar, L. Bichler, J. Szpunar, J. Alloys Compd. 789 (2019) 507–516.
[32] C.O.T. Galvin, M.W.D. Cooper, M.J.D. Rushton, R.W. Grimes, Nature Scientific Reports 6 (1–10) (2016) 36024.
[33] P.S. Ghosh, P.S. Somayajulu, A. Arya, G.K. Dey, B.K. Dutta, J. Alloys Compd. 638 (2012) 172–181.
[34] P.S. Somayajulu, P.S. Ghosh, A. Arya, K.V.V. Devi, D.B. Sathe, J. Banerjee, K.B. Khan, G.K. Dey, B.K. Dutta, J. Alloys Compd. 664 (2016) 291–303.
[35] M.W.D. Cooper, M.J.D. Rushton, R.W. Grimes, J. Phys. Condens. Matter 26 (1–10) (2014) 105401.
[36] M.W.D. Cooper, N. Kuganathan, P.A. Burr, M.J.D. Rushton, R.W. Grimes, C.R. Stanek, D.A. Andersson, J. Phys. Condens. Matter 28 (1–8) (2016) 405401.
[37] S.J. Plimpton, J. Comp. Phys. 117 (1995) 1–19.
[38] http://lammps.sandia.gov/.
[39] X.-Y. Liu, D.A. Andersson, B.P. Uberuaga, J. Mater. Sci. 47 (2012) 7367.
[40] X.W. Zhou, S. Aubry, R.E. Jones, A. Greenstein, P.K. Schelling, Phys. Rev. B 79 (2009), 115201(1)-(17).
[41] F. Muller-Plathe, J. Chem. Phys. 106 (1997) 6082–6085.
[42] J. Callaway, Phys. Rev. 113 (1959) 1046–1051.
[43] K. Gofryk, S. Du, C.R. Stanek, J.C. Lashley, X.-Y. Liu, R.K. Schulze, J.L. Smith, D.J. Safarik, D.D. Byler, K.J. McClellan, B.P. Uberuaga, B.L. Scott, D.A. Andersson, Nat. Commun. 5 (2014), 4551(1)-(7).
[44] M. Ali, P. Nagels, Phys. Status Solidi 21 (1967) 113–116.
[45] M.D. Mathews, B.R. Ambekar, A.K. Tyagi, J. Nucl. Mater. 280 (2000) 246–249.
[46] T. Yamashita, N. Nitani, T. Tsuji, H. Inagaki, J. Nucl. Mater. 245 (1997) 72–78.
[47] K. Govers, S. Lemehov, M. Hou, M. Verwerft, J. Nucl. Mater. 376 (2008) 66–77.
[48] S.I. Potashnikov, A.S. Boyarchenkov, K.A. Nekrasov, A.Ya Kupryazhkin, J. Nucl. Mater. 419 (2011) 217–225.
[49] J. Belle, R.M. Berman, Thorium Dioxide: Properties and Nuclear Application, U.S. DOE/NE-0060, Naval Reactors Office, Washington, DC, 1984.
[50] S. Dash, S.C. Parida, Z. Singh, B.K. Sen, V. Venugopal, J. Nucl. Mater. 393 (2009) 267–281.
[51] R.J.M. Konings, et al., J. Phys. Chem. Ref. Data 43 (2014) 1–95.
[52] J. Belle, R.M. Berman, Properties of Thoria and Thoria-Urania: A Review, *U.S. WAPD-TN-1340*, Westinghouse Electric Corporation, West Mifflin, Pennsylvania, 1978.
[53] A.C. Victor, T.B. Douglas, J. Phys. Chem. Ref. Data 43 (2014) 1–95.
[54] Y.S. Touloukian, in: R.W. Powell, C.Y. Ho, P.G. Klemens (Eds.), Thermal Conductivity: Nonmetallic Solids, *Thermophysical Properties of Matter*, vol. 2, IFI/Plenum, New York, 1970.
[55] K. Bakker, E.H.P. Cordfunke, R.J.M. Konings, R.P.C. Schram, J. Nucl. Mater. 250 (1997) 1–12.
[56] C. Cozzo, D. Staicu, J. Somers, A. Fernandez, R.J.M. Konings, J. Nucl. Mater. 416 (2011) 135–141.
[57] C.G.S. Pillai, P. Raj, J. Nucl. Mater. 277 (2000) 116–119.
[58] J. Belle, R.M. Berman, Thorium Dioxide: Properties and Nuclear Application, U.S. DOE/NE-0060, Naval Reactors Office, Washington, DC, 1984.
[59] R. Berman, Sci. Prog. 55 (1967) 357–377.
[60] G. Busker, A. Chroneos, R.W. Grimes, I.W. Chen, J. Am. Ceram. Soc. 82 (1999) 1553–1559.
[61] M.R. Tonks, X.-Y. Liu, D.A. Andersson, D. Perez, A. Chernatynskiy, G. Pastore, C.R. Stanek, R. Williamson, J. Nucl. Mater. 469 (2016) 89–98.